Journal of Computational Physics **169,** 624–651 (2001)
doi:10.1006/jcph.2000.6692, available online at http://www.idealibrary.com on IDEAL®

The Second Gradient Method for the Direct Numerical Simulation of Liquid–Vapor Flows with Phase Change

D. Jamet,* O. Lebaigue,* N. Coutris,*,† and J. M. Delhaye*

*Commissariat à l'Energie Atomique/Grenoble, Département de Thermohydraulique et de Physique; and †Institut National Polytechnique de Grenoble, Ecole Nationale Supérieure de Physique de Grenoble, Grenoble Cedex 9 38054, France
E-mail: didier.jamet@cea.fr; olivier.lebaigue@cea.fr

Received April 28, 2000

This paper presents a new method to simulate liquid–vapor flows with phase change using a phase-field-like approach. In this method, the liquid–vapor interface is described as a three-dimensional continuous medium across which physical properties have strong but continuous variations. This continuous variation is made possible by imposing that the internal energy of the fluid depends on its density gradient. This description, called the second gradient theory, is numerically attractive since a single system of partial differential equations (PDEs) is necessary to determine the flow in the entire two-phase system, the phase change, the displacement of the interfaces, and their change in topology being a part of their solution. However, to solve these PDEs using a reasonable number of grid points on a fixed grid, the interfaces need to be artificially enlarged. It is shown that this artificial enlargement can be thermodynamically consistent if the thermodynamic behavior of the fluid is modified within the binodal curve. The consequences of this thermodynamic modification are studied in detail. In particular it is shown that, within the frame of the second gradient theory, the interface thickness and the surface tension vary with the mass and heat fluxes across the interface and that these variations increase with the thickness of the interface. As a consequence, for a given accuracy, an upper bound exists for the interfacial heat and mass fluxes that can be simulated. Examples of applications in one and two dimensions show the potentialities of the method presented, in particular to deal with moving contact lines, the description of which is a part of the second gradient theory.

1. INTRODUCTION

Complex liquid–vapor flows with phase change are often encountered in industrial applications such as heat exchangers, nuclear reactors, boilers, etc. Their better understanding

0021-9991/01 $35.00

requires experimental investigations as well as the development of analytical models. Direct numerical simulations can be a way to help interpret experimental data and understand local physical phenomena that can then be used to develop analytical models. For that purpose, the use of the direct numerical simulation is already quite common in single-phase fluid dynamics. It is not yet the case in two-phase flows with phase change, because the numerical problems encountered to simulate such flows are much more complicated. The first issue that must be faced is the tracking of a surface of discontinuity on a fixed numerical grid. Several methods proved their efficiency to solve this problem; the most common ones are the volume-of-fluid (e.g., [22]), front-tracking (e.g., [36]), and level-set methods (e.g., [34]). Nevertheless, these methods mainly deal with immiscible fluid systems. Indeed, in such flows, the speed of displacement of an interface is equal to the velocity of the fluids (gas and liquid) at the interface. Therefore, knowing the velocity field, it is quite easy to interpolate it at the interface and move the interface accordingly. When phase change exists, the problem is more complicated because three different velocities exist at an interface: the velocities of the liquid and vapor phases and the speed of displacement of the interface. The interpolation procedure is then no longer trivial. Juric [18, 19] showed that it was nevertheless possible to determine the speed of displacement of an interface in such a case by using an iterative procedure to satisfy a Clapeyron's relation at the interface, and he applied this procedure to the front-tracking method. More recently, this method has been applied to the volume-of-fluid method [38].

In all the methods using a fixed grid on which the interfaces of the system move (the group to which the methods previously cited belong) the concept of continuous surface tension (CSF) is used (e.g., [3]). Since the equations of motion of the two-phase system are solved on a fixed grid and since in general the interface does not intersect the grid points, surface tension must be transformed into a volumetric force. More generally, for numerical reasons, the interface is spread on the fixed mesh and the equations of motion are then solved for variables that vary continuously across three-dimensional interfacial zones thus numerically created.

In this paper, we want to study how far one can go using this concept of a three-dimensional continuous interfacial zone that is numerically convenient to simulate liquid–vapor flows with phase change: instead of dealing with discontinuities, one deals with smooth variations, which is numerically simplex. This kind of approach, generally called the phase-field method, has recently become popular, as shown in [1] for its applications in fluid mechanics. The starting point is the following: if equations of motion have to be written for continuous variables, these equations should be derived by using general physical principles, which should preserve the physical coherence of the model used within interfacial zones. Since the nineteenth century, it is known (at least for equilibrium states) that a liquid–vapor interface can be described as a three-dimensional continuous medium using the so-called van der Waals, Cahn–Hilliard, or second gradient theory, the last being briefly presented in Section 2. This theory, in which it is assumed that the internal energy of the fluid depends not only on its entropy and density but also on its density gradient, ensures a perfect thermodynamic consistency of the equations describing the motion of a fluid within a liquid–vapor interfacial zone. It must be noted that a similar theory is currently extensively applied to simulate solidification problems and has given rise to the so-called phase-field models. These methods have already been applied to study many problems such as dendrites (e.g., [39]), binary alloys (e.g., [2]), and anisotropic interfaces (e.g., [24]) for instance. One of the main reference papers to these methods is [27], in which it is stated that, for the temperature and

the energy may be independent variables, the appropriate thermodynamic potential must no longer be the free energy but rather the entropy. Therefore, it is stated that the entropy depends not only on an "order parameter C," but also on its gradient. In this paper, it is shown that, for liquid–vapor systems, a complete system of balance equations, consistent with the second principle of thermodynamics, can be found by replacing the free energy, not by the entropy, as in the phase-field models, but rather by the internal energy. The order parameter is then the fluid density, which has a clear physical meaning. To our knowledge no attempt has been made to model liquid–solid systems for which the order parameter would be the entropy, which then would have a clear physical meaning, and the thermodynamic potential would be the internal energy.

The second gradient theory is *a priori* dedicated to describe physical liquid–vapor interfaces and is therefore generally used to study physical systems close to the critical point, where the interface thickness is relatively large. A review of these kinds of applications can be found in [1]. However, for more common applications, the temperature of a system is not close to the critical temperature of the fluid and the liquid–vapor interfaces are therefore very thin, i.e., of the order of a few Ångströms. If this theory had to be used just as it is, the grid spacing should be of the order of a few Ångströms, which means that about one hundred million points regularly spaced would be necessary to solve a one-dimensional problem which is only one centimeter long. That would be of course of no interest. The theory must therefore be adapted such that the thermodynamic coherence of the equations of motion of a fluid within the interfacial zones is maintained while the interfacial thickness is artificially enlarged, so that a standard grid can capture it. It is shown in Section 3 that such an adaptation is possible but requires a modification of the thermodynamic behavior of a fluid inside the interfacial zone, or more precisely inside the binodal region. It must be noticed that this kind of approach has already been successfully used for immiscible fluids [14], but it appears that liquid–vapor phase change makes the problem more complicated, as will be discussed in Section 3.

Since the thermodynamic behavior of the fluid is modified for numerical purposes, it must be ensured that important macroscopic properties are not modified too much. This study is made in Section 4. In particular, it is shown that the values of the radius of the inclusions (bubbles or drops) and the interfacial mass fluxes as well as the interfacial heat fluxes that can be correctly simulated are limited. It is our current understanding that these limitations are the inherent consequences of the thermodynamically consistent model used and would therefore be difficult to eliminate. These limits are however clearly known. In Section 5 applications in one and two dimensions are presented using the method proposed. In these applications, phase change always occurs, at least locally, even though some of the systems are isothermal (in these cases, phase change is driven by local depressurization). Indeed, in the frame of the second gradient theory, phase change cannot be eliminated (unless the latent heat of evaporation is set to infinity, which has not been considered in this work). Section 6 presents some conclusions and perspectives to this work.

2. INTRODUCTION TO THE SECOND GRADIENT THEORY

Classically, at a macroscopic scale, an interface between a liquid and its vapor, and more generally between two fluids, is modeled as a surface of discontinuity endowed with properties, the most important of which being surface tension (e.g., [9]). However, at a microscopic scale, an interface is a volumetric transition zone across which the molecule

density for instance varies continuously. Therefore, it would be satisfactory to describe a liquid–vapor system, including the interfaces, by the general equations of fluid mechanics. The simplest way to determine such equations is to consider that the internal energy of the fluid depends not only on its entropy and density but also on its density gradient. Indeed, van der Waals [37] first showed that to model an interface as a three-dimensional continuous medium, the energy of a fluid particle must depend not only on its density (if it is assumed that the fluid is at thermal equilibrium) but also on its density gradient,

$$F = F^0(\rho) + \lambda \frac{(\nabla \rho)^2}{2}, \tag{1}$$

where F is the volumetric free energy of the fluid, F^0 is its classical part, and λ is the capillary coefficient, generally assumed to be constant.

This dependence on the density gradient explains the existence of a finite thickness of an interface as well as the existence of a surface tension.

Korteweg [21] later showed that the general constraint within a liquid–vapor interfacial zone also depends on the density gradient. Cahn and Hilliard studied interfaces at equilibrium separating fluids of different natures [4] using the same concept of an energy dependence on a general phase-indicator function.

2.1. *Thermodynamic Modeling*

Rocard [30] for instance clearly showed that the form of the free energy given by (1) can be explained at the molecular scale by using a mean field theory. Indeed, within a liquid–vapor interfacial zone, the density of particles surrounding a test particle no longer has a spherical symmetry and making a Taylor expansion of order one of this density of particles in the direction normal to the interface, one shows that to the "classical" interaction energy depending only on the density must be added an energy proportional to the square of the density gradient as postulated in Eq. (1). Such a fluid is said to be *endowed with internal capillarity*. Hence, it clearly appears that the introduction of a dependence of the energy of a fluid on its density gradient corresponds to a higher order modeling of it (as it is done in a Chapman–Enskog expansion in gas dynamics, for instance by Reese *et al.* [29]).

The equilibrium state of a fluid endowed with internal capillarity is such that its free energy is minimum. For a one-dimensional problem in a Cartesian system of coordinates, one then has

$$\delta \int_{z-}^{z+} \left[F^0(\rho) + \lambda \left(\frac{d\rho}{dz} \right)^2 + L_1 \rho \right] dz = 0, \tag{2}$$

where L_1 is a Lagrange multiplier accounting for the constraint that the system is closed, i.e., its mass is imposed.

Therefore, the density profile $\rho(z)$ at equilibrium must satisfy the differential equation

$$\lambda \frac{d^2\rho}{dz^2} = \mu(\rho) - L_1, \tag{3}$$

where μ is the chemical potential. L_1 is thus interpreted as the chemical potential at saturation.

Using this density profile at equilibrium, it can then be shown that the expression of the energy concentrated at the interface (sometimes called the excess energy), which is the surface tension, is given by

$$\sigma = \int_{z-}^{z+} \lambda \left(\frac{d\rho}{dz} \right)^2 dz. \tag{4}$$

The thermodynamic theory presented above for an isothermal system can be extended to a nonisothermal system, for which it is assumed that the internal energy of the fluid depends not only on its density and entropy, but also on its density gradient:

$$u = u(s, \rho, (\nabla\rho)^2). \tag{5}$$

Note that this model can be extended by accounting for a dependence on the entropy gradient. However, no clear consequence of this other dependence could justify its introduction to simulate the physical phenomena that are the subject of this study.

2.2. *Equations of Motion of a Fluid Endowed with Internal Capillarity*

So far, a thermodynamic description of a fluid endowed with internal capillarity has been given. Equations of motion of such a fluid have then to be derived. Several approaches are possible and are discussed in [33]. The details of their derivation can be found in [6] for a Hamiltonian approach and in [15] for a derivation using the principle of virtual work. It is found that the partial differential equations which govern the motion of a fluid endowed with internal capillarity are then

$$\frac{\partial \rho}{\partial t} + \nabla \cdot (\rho \boldsymbol{V}) = 0, \tag{6}$$

$$\rho \frac{d\boldsymbol{V}}{dt} = \boldsymbol{F} - \nabla p - \nabla \cdot (\lambda \nabla\rho \otimes \nabla\rho) + \nabla \cdot \boldsymbol{\tau}^D, \tag{7}$$

$$\rho \frac{de}{dt} = \boldsymbol{F} \cdot \boldsymbol{V} + \nabla \cdot ((-p\boldsymbol{I} - \lambda \nabla\rho \otimes \nabla\rho + \boldsymbol{\tau}^D) \cdot \boldsymbol{V}) + \nabla \cdot \left(\lambda \nabla\rho \frac{d\rho}{dt} \right) - \nabla \cdot \boldsymbol{q}, \tag{8}$$

where p is a pressure (defined by (9)), λ is the capillary coefficient (defined by (10)), $\boldsymbol{\tau}^D$ is the dissipative part of the stress tensor, e is the specific total energy, $\boldsymbol{q}$ is the heat flux, and

$$p \hat{=} \rho^2 \left(\frac{\partial u}{\partial \rho} \right)_{s,(\nabla\rho)^2} - \rho \nabla \cdot (\lambda \nabla\rho) \tag{9}$$

$$\lambda \hat{=} 2\rho \left(\frac{\partial u}{\partial (\nabla\rho)^2} \right)_{s,\rho}. \tag{10}$$

This system needs to be closed by giving the expressions for the specific internal energy $u(s, \rho, (\nabla\rho)^2)$ (since p and λ depend on u), the dissipative tensor $\boldsymbol{\tau}^D$, and the heat flux $\boldsymbol{q}$. The expression for the specific internal energy and its consequences will be studied in the next sections. By using the thermodynamics of irreversible processes, Seppecher [32] gave a general expression for $\boldsymbol{\tau}^D$ and $\boldsymbol{q}$, and five coefficients appear in the expression of $\boldsymbol{\tau}^D$, for instance. Since the physical significance of all these coefficients is to our knowledge not firmly established, we keep a Newtonian expression for $\boldsymbol{\tau}^D$ (an assumption which is

generally made and which gives good interpretations of macroscopic phenomena as shown in [33] for instance). Similarly, we keep a classical Fourier's law for the heat flux.

Hence,

$$\boldsymbol{\tau}^D = \nu \operatorname{tr}(\boldsymbol{D}) + 2\mu \boldsymbol{D}, \tag{11}$$

where $\boldsymbol{D} \hat{=} (\nabla \boldsymbol{V} + \nabla^T \boldsymbol{V})/2$ and

$$\boldsymbol{q} = -k \nabla T. \tag{12}$$

The fact that the Cahn–Hilliard theory accounts for surface tension as a volumetric property has already been shown in Section 2.1 where surface tension has been interpreted as an energy per unit area. Given the momentum balance equation (7), an analysis of the efforts applied on a elementary volume placed within an interfacial zone shows (e.g., [16]) that *at equilibrium* the pressure in the tangential direction of the interface is weaker than in the normal direction. A tension is thus applied in the tangential direction of an interface, the integration of which is interpreted as surface tension. The expression thus found is (4).

2.3. *Some Important Comments*

The system of Eqs. (6)–(8) has been established for an interfacial zone, where the density gradient has a nonnegligible contribution to their energy. However, within the phases this contribution can be neglected and it is straightforward to show that in that case Eqs. (6)–(8) reduce to the classical equations of motion of a single-phase fluid.

That means that *solving only these three continuous partial differential equations will determine the whole liquid–vapor two-phase flow, with the movement of the interfaces, including breakup and coalescence phenomena, being just a part of the solution.* Therefore, virtually no particular treatment of the interfaces is needed, which means that the main difficulty encountered in numerical methods dedicated to the direct numerical simulation of two-phase flows could be overcome.

However, if one wants to benefit from this virtual advantage, a difficulty must previously be resolved. Indeed, a simple analysis of orders of magnitudes (e.g., [7]) shows that the relevant length scale associated with the equation of motion of a fluid endowed with internal capillarity is about 10^{-10} m. Since surface tension appears as an integral property, the interfacial zones must be numerically resolved, and therefore several discretization points should be used to capture an interface. Hence, to solve a one-dimensional problem which is 1 mm long, about 10,000,000 discretization points uniformly spaced are needed, which is absolutely impossible and of no interest.

A way to overcome this issue is presented in the next section.

3. MODIFICATION OF THE THERMODYNAMIC BEHAVIOR OF A FLUID

The question to which we will give an answer in this section is: *is it possible to artificially enlarge a liquid–vapor interfacial zone without losing the thermodynamic coherence of the second gradient model?*

3.1. *The Vicinity of the Critical Point*

The vicinity of the critical point is particularly appropriate to the application of the second gradient theory. Indeed, let us consider a liquid–vapor system at equilibrium at a

temperature slightly different and lower than the critical temperature T_c of a fluid. Under these conditions, the thickness of a liquid–vapor interface is typically of the order of one micrometer. That means that close to the critical point, the use of a three-dimensional model to describe a liquid–vapor interface is fully justified, which is the reason this model is mainly used to study critical phenomena (e.g., [11]).

Furthermore, in the vicinity of the critical point, simplifications of the equation of state of a fluid can be made [31]. For instance, it can be shown that the dependence on the energy W defined as

$$W(\rho) \hat{=} F(\rho) - \left(F\left(\rho_v^{sat}\right) + \mu^{sat}\left(\rho - \rho_v^{sat}\right)\right), \tag{13}$$

where μ^{sat} is the chemical potential at saturation, ρ_v^{sat} and ρ_l^{sat} are the densities of the vapor and liquid phases at saturation respectively, and A is a "constant" (all these properties are functions of the temperature), takes the following particularly simple form:

$$W(\rho) = A\left(\rho - \rho_v^{sat}\right)^2\left(\rho - \rho_l^{sat}\right)^2. \tag{14}$$

Consider a plane interface at equilibrium in the vicinity of the critical point. Assuming that the capillary coefficient is constant, the momentum balance equation can be integrated analytically and it is found that the density profile across a plane interface at equilibrium is

$$\rho(z) = \frac{\rho_l^{sat} + \rho_v^{sat}}{2} + \frac{\rho_l^{sat} - \rho_v^{sat}}{2}\tanh\left(z\frac{\rho_l^{sat} - \rho_v^{sat}}{\sqrt{2\lambda/A}}\right). \tag{15}$$

Under these conditions, the interface thickness and of the surface tension are given by

$$h = \frac{4}{\rho_l^{sat} - \rho_v^{sat}}\sqrt{\frac{\lambda}{2A}}, \tag{16}$$

$$\sigma = \frac{\left(\rho_l^{sat} - \rho_v^{sat}\right)^3}{6}\sqrt{2A\lambda}. \tag{17}$$

Equations (16) and (17) show that the second gradient theory predicts that in the vicinity of the critical point, the thickness of an interface at equilibrium is proportional to $\sqrt{\lambda/A}$ and its surface tension is proportional to $\sqrt{\lambda A}$. This remark will be important to better understand the way an interface can be artificially enlarged.

This is done in the following section.

3.2. *Artificial Enlargement of an Interface: Main Idea*

We recall that our main purpose is to artificially enlarge an interface so that a standard mesh can capture it. The thickness of an interface is then a parameter, whose value must *a priori* be given following numerical arguments (size of the system studied, computer power, etc.).

The study of an interface at equilibrium in the vicinity of the critical point, presented in Section 3.1, indicates that the thickness of such an interface is proportional to $\sqrt{\lambda}$. Hence, an artificial enlargement can be achieved by increasing λ. However, its surface tension is also proportional to $\sqrt{\lambda}$ and therefore, increasing the capillary coefficient will increase the value of the surface tension of the fluid. This is not acceptable since our main goal is to perform direct numerical simulations for which surface tension is an important physical property.

This issue can be overcome by decreasing the value of the coefficient A at the same rate as λ is increased (see Eqs. (16) and (17)). Hence, *the thickness of an interface can be increased, without changing the value of surface tension*.

These considerations show that it should be possible to artificially enlarge an interface without modifying the thermodynamic coherence of the second gradient model provided that the thermodynamic behavior of the fluid is modified inside the interfacial zone, or more precisely, if the dependence on the density of the thermodynamic functions are modified for density values between the values of the densities at saturation, that is, inside the binodal region.

Another issue is then encountered. Indeed, modifying the value of A modifies the thermodynamic behavior of the fluid for all the values of the density as shown by relation (14). In particular, the derivative $(dP/d\rho)$ will be modified at the phase densities at saturation, which means that the speed of sound of the liquid and vapor phases will be modified. This is not acceptable if the goal is to perform direct numerical simulations.

The crux is then to modify the equation of state of the fluid so that the interface can be artificially enlarged, but maintaining a certain regularity near the binodal curve, i.e., for values of ρ closed to ρ_v^{sat} and ρ_l^{sat}.

A full solution to this problem is presented in the next section.

It must be emphasized that this latter issue makes the problem of using a diffuse interface method to simulate phase-change phenomena more difficult than to simulate immiscible two-phase flows. Indeed, Jacqmin [13, 14] developed the same idea as the one presented above but for immiscible fluids for which the Cahn–Hilliard theory is used.[1] The issue of maintaining the equation of state of the bulk phases does not exist in that case, since the phases are supposed to be incompressible.

3.3. *Artificial Enlargement of an Interface: Mathematical Implementation*

The best way to find the thermodynamic behavior of a fluid that would satisfy all the conditions that must be recovered is to work directly on the "classical" free energy of the fluid and on its capillary coefficient supposed to be constant (or a function of the temperature only). The reason is that once the thermodynamic behavior is given, we have shown in Section 3.1 that all the interfacial properties are just consequences.

Let us first list the conditions that must be satisfied:

- The value of the thickness of an interface at equilibrium h^{sat} can be chosen arbitrarily (from numerical arguments).
- The value of the surface tension at equilibrium σ^{sat} can be chosen arbitrarily (from experiment).
- The bulk phase thermodynamic properties can be chosen arbitrarily (from experiment or models).
- The pressure as a function of density must be once continuously differentiable (continuous speed of sound).

It is proposed to search for the modified thermodynamic function $W^{mod}(\rho)$ using

$$W^{mod}(\rho) = \frac{\sigma^{sat}}{h^{sat}}(\phi(r))^2, \tag{18}$$

[1] Note that in the case of immiscible fluids a color function C (which has a value of one in a phase and zero in the other) is used as the phase parameter, the density being the phase parameter in our case.

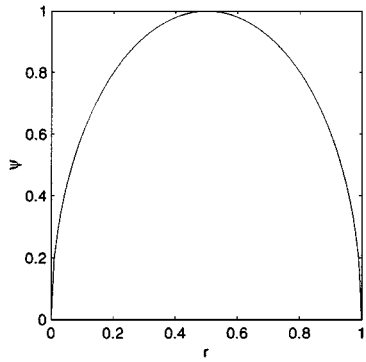

FIG. 1. Shape of the function $\psi(r)$ for water at 1 K below the critical point and an artificial thickness of an interface at equilibrium equal to 1 mm.

where ϕ is a nondimensional function of the nondimensional variable $r \hat{=} (\rho - \rho_v^{sat})/(\rho_l^{sat} - \rho_v^{sat})$.

Let us define the function $\psi(r)$ as

$$\psi(r) \hat{=} \frac{\phi(r)}{\max(\phi)}. \tag{19}$$

Jamet [15] showed that the shape of the function $\psi(r)$ *must* be the one shown on Fig. 1.

This shape is easily understood. It has been shown in Section 3.2 that one of the main requirements that must be satisfied to enlarge an interface is to decrease the value of A in the vicinity of the critical point, or more generally to decrease the maximum of the function $W(\rho)$. If that were the only requirement, then the function $\psi(r)$ would still have a parabolic shape. However, it is moreover required that the function $(dP/d\rho)(\rho)$ keep its value and be continuous at $\rho = \rho_v^{sat}$ and $\rho = \rho_l^{sat}$. It is straightforward to show that this derivative is linked to the derivative of $\sqrt{W}(\rho)$. Therefore, the derivative of $\sqrt{W}(\rho)$ must be kept constant and its maximum must be decreased. If this decrease is huge, typically of the order of 10,000 in the conditions of the Fig. 1, then the initially parabolic shape of $\sqrt{W}(\rho)$ will be drastically shrunk only in its medium part, and its tangents at $\rho = \rho_v^{sat}$ and $\rho = \rho_l^{sat}$ will be kept constant, so that its dimensionless form $\psi(r)$ *must* be the one shown on Fig. 1.

Given the function $\psi(r)$, all the thermodynamic properties of the fluid, such as the pressure for instance, can be deduced by derivation. For instance, it can be shown that

$$P^{mod}(\rho) - P^{sat} = \frac{2\sigma^{sat}}{h^{sat}}\phi\left(\frac{\rho}{\rho_l^{sat} - \rho_v^{sat}}\frac{d\phi}{dr} - \frac{1}{2}\phi\right). \tag{20}$$

Figure 2 shows the modified equation of state for water at 1 K below the critical point for an artificial thickness of an interface at equilibrium arbitrarily equal to 1 mm. For the sake of simplicity, it has been assumed that the van der Waals' equation of state is valid in the bulk phases and is plotted inside the binodal region as a reference equation of state. It can be seen that the modification of the equation of state is really drastic within the binodal region. The reason is that in the case considered here, the artificial enlargement of the interface thickness is of the order of 10,000, which corresponds to a decrease of the maximum of $(dP/d\rho)$ (achieved in the middle of the binodal region) of about 10,000 (see Eqs. (16) and (17) for which A is roughly proportional to $\max(dP/d\rho)$).

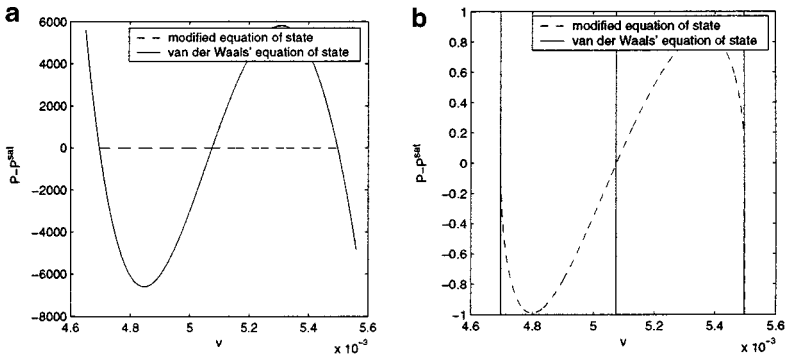

FIG. 2. Modified van der Waals' equation of state $P(v)$ for water at 1 K below the critical point such that the artificial thickness of an interface is equal to 1 mm. (a) van der Waals' and modified equations of state for which the pressure scale is adapted to the van der Waals' equation of state. (b) van der Waals' and modified equations of state for which the pressure scale is adapted to the modified equation of state.

The procedure described above to find the modified thermodynamic behavior of a fluid is valid if the system is isothermal: the function $\psi(r)$ and then the modified volumetric free energy $F^{mod}(\rho)$ can be found for any given temperature. However, Jamet [15] showed that *working directly with the free energy to seek a modified thermodynamics keeps the whole thermodynamic coherence of the model and that Maxwell's thermodynamic relations are recovered*.

It must be emphasized that the modified thermodynamics presented above does not change the values of the densities at saturation, which means that the binodal curve is not modified. Therefore, *any thermodynamic function is unchanged at saturation*, and particularly the specific enthalpy i. *The latent heat of vaporization* $\mathcal{L}$ defined as

$$\mathcal{L} \hat{=} i_v^{sat} - i_l^{sat} \tag{21}$$

is therefore not modified by the modified thermodynamics proposed here.

4. SOME CONSEQUENCES OF THE MODIFICATION OF THE THERMODYNAMIC BEHAVIOR OF A FLUID

The purpose of this section is to study the physical consequences introduced by the drastic modification of the equation of state necessary to artificially enlarge an interface as shown in Section 3.

4.1. *Radius of Inclusions That Can Be Simulated*

According to Laplace's theory of capillarity, the pressures of the phases surrounding an inclusion of radius R at equilibrium are given by (e.g., [5])

$$P_v - P^{sat} = \eta \frac{\rho_v^{sat}}{\rho_l^{sat} - \rho_v^{sat}} \frac{2\sigma}{R} \tag{22}$$

and

$$P_l - P^{sat} = \eta \frac{\rho_l^{sat}}{\rho_l^{sat} - \rho_v^{sat}} \frac{2\sigma}{R}, \tag{23}$$

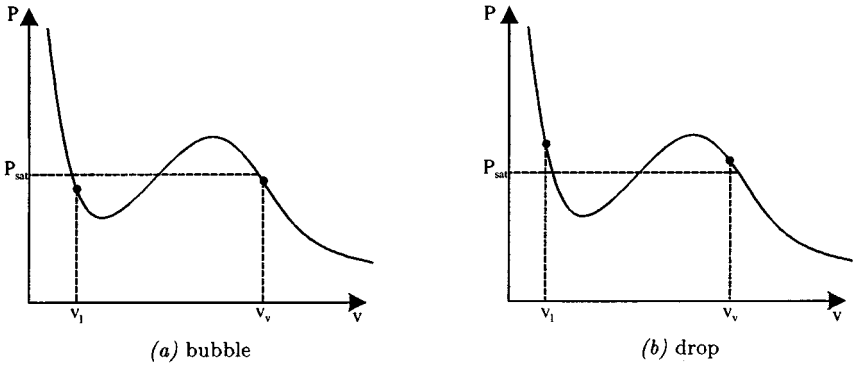

FIG. 3. Characteristic points of the liquid and vapor phases of a bubble and a drop in a Clapeyron diagram.

where

$$\eta \hat{=} \begin{cases} +1 & \text{for a droplet} \\ -1 & \text{for a bubble.} \end{cases} \tag{24}$$

As shown in Fig. 3, these pressures are such that one of the phases is metastable, i.e., located in the binodal region, where the equation of state is modified. Therefore the relations (22) and (23) may not be verified and the Laplace relation is likely to be violated for a modified equation of state.

The equilibrium state of a spherical inclusion described by the second gradient theory is such that (e.g., [10])

$$P_l - P_v = 2 \int_0^\infty \lambda \frac{(d\rho/dr)^2}{r}\, dr. \tag{25}$$

This relation is general and, if the radius of the inclusion is greater than the interface thickness ([15]), is the Laplace relation. *The Laplace relation is therefore not violated by the modified equation of state introduced in Section 3*.

Moreover, since the modified thermodynamics considered in Section 3 is such that the function $(dP/d\rho)(\rho)$ is continuous, especially on the binodal curve, an analysis based on Taylor expansions of order one in $(2\sigma/R)$ shows that *Eqs. (22) and (23) are satisfied for any modified thermodynamics*. The influence of the modification of the equation of state appears only if the Taylor expansions are made up to an order three,

$$P_{l,v}^{mod} - P_{l,v} = \xi^{sat} \left(\frac{2\sigma}{R} \right)^3, \tag{26}$$

where

$$\begin{cases} \xi^{sat} \hat{=} \eta \dfrac{\rho_l^{sat} \rho_v^{sat}}{6\rho_p^{sat} \left(\rho_l^{sat} - \rho_v^{sat}\right)^4} \dfrac{\dfrac{d^2\mu^{mod}}{d\rho^2}\left(\rho_p^{sat}\right) - \dfrac{d^2\mu}{d\rho^2}\left(\rho_p^{sat}\right)}{\left(\dfrac{d^2\mu}{d\rho^2}\left(\rho_p^{sat}\right)\right)^3} \\ \rho_p^{sat} \hat{=} \dfrac{\left(\rho_l^{sat} - \rho_v^{sat}\right) - \eta\left(\rho_l^{sat} + \rho_v^{sat}\right)}{2} \end{cases} \tag{27}$$

and $P_{l,v}$ is the pressure in either the liquid or the vapor phase for nonmodified thermodynamics, and $P_{l,v}^{mod}$ is this pressure for a modified equation of state.

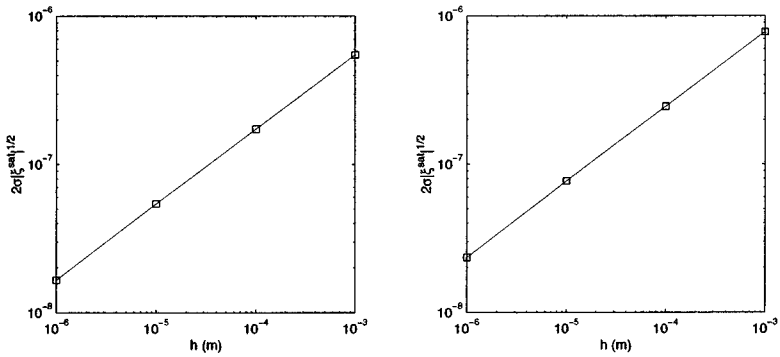

FIG. 4. Typical values of 2σ for water at 30 K below the critical point for different values of the artificial thickness of an interface at equilibrium.

Let us suppose that, for any reason, it is acceptable to make an error $\epsilon < \epsilon_{lim}$ on the absolute pressure level, where ϵ is defined as

$$\epsilon \hat{=} \left| \frac{P_{l,v}^{mod} - P_{l,v}}{2\sigma/R} \right|. \tag{28}$$

Equations (26) and (28) show that inclusions whose radii are greater than a limit R_{lim} given below will introduce an error ϵ less than ϵ_{lim}.

$$R_{lim} = 2\sigma \sqrt{|\xi^{sat}|} \frac{1}{\sqrt{\epsilon_{lim}}}. \tag{29}$$

Typical values of $2\sigma\sqrt{|\xi^{sat}|}$ for water are plotted in Fig. 4 for different values of the temperature and of the artificial interface thickness at equilibrium. This figure shows that if, for example, ϵ_{lim} is equal to 10^{-4} and if the artificial interface thickness is equal to 0.1 mm at 1 K below the critical point, then the radius of the inclusions that will satisfy the criterion (i.e., $\epsilon < 10^{-4}$) must be greater than about 1 mm. For radii smaller than 1 mm, the pressure level surrounding the interface will not satisfy the criterion on ϵ, even though Laplace's relation will always be satisfied.

4.2. *Interfacial Mass Fluxes That Can Be Simulated*

The issue that will be handled in this section is *to know whether the thermodynamics modification introduced in Section 3 modifies the speed of displacement of an interfacial zone during a phase-change process*.

For this purpose, *a stationary, one-dimensional, isothermal problem* is studied. Such a problem corresponds to the physical situation sketched in Fig. 5. Note that *phase change exists even though the system is isothermal*. Physically speaking, phase change in this case is due to depressurization: as the piston is withdrawn, the vapor pressure decreases and the liquid and vapor phases are no longer in thermodynamic equilibrium. To recover thermodynamic equilibrium, some liquid must vaporize. This vaporization consumes energy that is transported toward the interface *via* conductive heat fluxes. These heat fluxes need nonzero temperature gradients. In this section, it is assumed that the thermal conductivity is

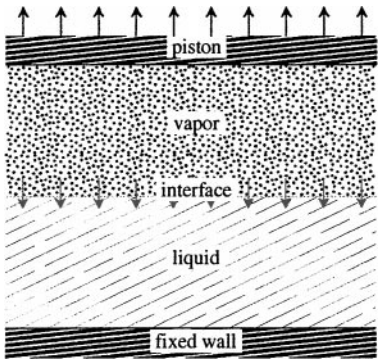

FIG. 5. Sketch of a one-dimensional isothermal phase-change problem.

large, the phase change is slow, and the phases can be considered isothermal. The detailed conditions under which this asumption is valid can be found in [15].

If the piston and wall velocities are constant then the speed of displacement of the interface is constant and given by mass conservation (e.g., [9]):

$$V^i = \frac{\rho_l V_l - \rho_v V_v}{\rho_l - \rho_v} \tag{30}$$

The bulk densities ρ_l and ρ_v are thus such that (e.g., [12])

$$\begin{cases} P(\rho_v) = P^{sat} - \frac{\dot{m}_c^2}{2}\left(\frac{1}{\rho_v^{sat}} - \frac{1}{\rho_l^{sat}}\right) \\ P(\rho_l) = P^{sat} + \frac{\dot{m}_c^2}{2}\left(\frac{1}{\rho_v^{sat}} - \frac{1}{\rho_l^{sat}}\right), \end{cases} \tag{31}$$

where

$$\dot{m}_c \hat{=} \rho_l(V_l - V^i) = \rho_v(V_v - V^i). \tag{32}$$

Equations (31) show that the liquid and the vapor are respectively subcooled and superheated; the phase characteristic points are therefore located outside the binodal curve.

This one-dimensional, isothermal, stationary problem (in the frame of reference of the interface) can be studied using the second gradient model and it is found that the pressures of the phases are given by

$$\begin{cases} P(v_l) - [P(v_v) - \dot{m}^2(v_l - v_v)] = 0 \\ \int_{v_l}^{v_v} \{P(v) - [P(v_v) - \dot{m}^2(v - v_v)]\}\, dv = 0, \end{cases} \tag{33}$$

where $v \hat{=} 1/\rho$ is the specific volume and $\dot{m} \hat{=} \rho V = const.$

Equations (33) is a generalization of the Maxwell's rule [23] in the presence of an interfacial mass transfer (e.g., [7]). It must be emphasized that these relations are satisfied whatever the equation of state $P(v)$.

A Taylor expansion of order one in $\dot{m}^2$ of Eq. (33) can be made [15] which leads exactly to the relations (31) (in which $\dot{m}_c$ is replaced by $\dot{m}$). Since these relations imply that the phases are not metastable, *any artificial enlargement of an interface does not modify the bulk*

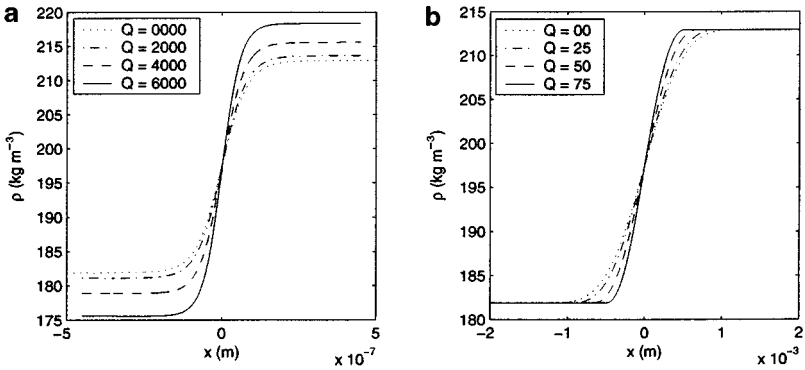

FIG. 6. Evolution of density profiles with the interfacial mass flux (in kg m^2 s^{-1}) for water at 1 K below the critical point. (a) Van der Waals' thermodynamics. Note the symmetric effect of the recoil pressure on phase densities. (b) Modified thermodynamics such that the artificial thickness of an interface at equilibrium is equal to 1 mm.

phase densities. Back in an absolute frame of reference, since the piston and wall velocities V_v and V_l are parameters of the problem, *the speed of displacement of the interface given by (30) is not modified by its artificial enlargement*.

Casal and Gouin [7] showed that the second gradient theory predicts a variation of surface tension with the interfacial mass flux, and the issue is then to know how an artificial enlargement modifies such a variation.

Figure 6 shows interface density profiles at 1 K below the critical point crossed by different mass fluxes for a van der Waals' equation of state and for a modified equation of state. This figure shows that in the case of a modified equation of state, the interface thickness is more sensitive to an interfacial mass flux than in the case of a van der Waals' equation of state. This increased sensitivity has two drawbacks: first, if the mass flux is too high, the interface thickness will no longer be captured and second, an induced variation of the surface tension could corrupt the physical relevance of a simulation.

Taylor expansions to first order in $\dot{m}^2$ of the density profile show that the interface thickness and the surface tension are given by the approximations [15]

$$\frac{h-h^{sat}}{h^{sat}} \simeq -\dot{m}^2 h^{sat} \frac{\left(\rho_l^{sat}-\rho_v^{sat}\right)^2}{4\sigma^{sat}\rho_l^{sat}\rho_v^{sat}\left(\rho_l^{sat}+\rho_v^{sat}\right)} \tag{34}$$

and

$$\frac{\sigma-\sigma^{sat}}{\sigma^{sat}} \simeq \dot{m}^2 h^{sat} \frac{\left(\rho_l^{sat}-\rho_v^{sat}\right)^2}{4\sigma^{sat}\rho_l^{sat}\rho_v^{sat}\left(\rho_l^{sat}+\rho_v^{sat}\right)}. \tag{35}$$

The linear variation with the interface thickness explains the difference between the profiles of Figs. 6a and 6b.

Equations (34) and (35) must help to decide whether the method proposed can be used to perform a relevant numerical simulation. Let us suppose for instance that, for any reason, it is acceptable to make a relative error in the value of the surface tension of 1%. At 1 K below the critical point, this means that the interfacial mass flux must be lower than 7 kg m^2 s^{-1}, which corresponds to a piston velocity equal to about 5.4 mm s^{-1} for the problem

sketched in Fig. 5. If this value is considered to be too small for the physical parameters used in the desired numerical simulation, the only solution is to change the mesh size so that the artificial interface thickness can be decreased.

4.3. *Interfacial Heat Fluxes That Can Be Simulated*

When a liquid–vapor interface is modeled as a discontinuous surface, it is generally assumed that the temperature at the interface is equal to the saturation temperature. In the second gradient theory, the temperature in the interfacial zone is given by the solution of (6)–(8) and the issue is therefore *to know whether the temperature within an interfacial zone is at least close to the saturation temperature*.

Let us consider *a one-dimensional liquid–vapor system under mechanical equilibrium in which the vapor phase is superheated by a temperature* ΔT *and the liquid phase is subcooled by the same temperature* ΔT (see Fig. 7). The density profile should thus be such that the interfacial zone is automatically located where the saturation temperature is reached.

This problem requires solving the momentum and energy balance equations (see Eqs. (7) and (8))

$$\frac{dP}{dz} = \lambda\rho\frac{d^3\rho}{dz^3} \tag{36}$$

$$\frac{d}{dz}\left(k\frac{dT}{dz}\right) = 0, \tag{37}$$

where the capillary coefficient λ is assumed to be constant and k is the thermal conductivity *a priori* function of ρ.

The coupling between Eqs. (36) and (37) is mainly encountered through the dependence of the pressure on the temperature, that is, through the equation of state of the fluid which is likely to be modified as described in Section 3.

Typical density and temperature profiles for a van der Waals' equation of state as well as for a modified equation of state are shown in Fig. 8. In both cases, it can be seen that *the saturation temperature is reached within the interfacial zone.*

However, *when the heat flux is increased through an increase of the temperature difference* ΔT*, Fig. 9 shows that the interface thickness varies, which implies also a variation of the surface tension.*

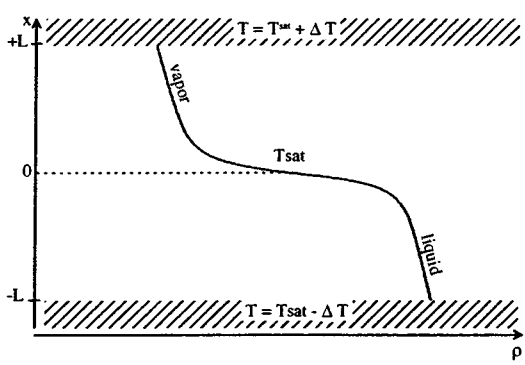

FIG. 7. Sketch of a one-dimensional heat transfer across a liquid–vapor interfacial zone at mechanical equilibrium.

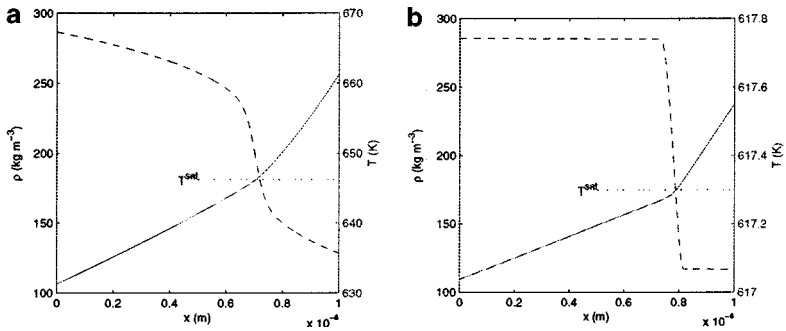

FIG. 8. Density and temperature profiles across a liquid–vapor interface at mechanical equilibrium crossed by a constant heat flux. (a) Van der Waals' equation of state. (b) Modified equation of state for which the thickness of an interface at equilibrium is equal to 10^{-4} m.

A first attempt to explain this variation can be found in [15], where it is assumed that the temperature gradient is constant (i.e., $k = const$). This attempt is based on a Taylor expansion of order one in ΔT and leads to the approximations

$$\frac{h - h^{sat}}{h^{sat}} \simeq -\nabla T (h^{sat})^2 \frac{\rho_l^{sat} + \rho_v^{sat}}{2} \frac{\rho_v^{sat} \mathcal{L}}{2T^{sat}\left(\rho_l^{sat} - \rho_v^{sat}\right)\sigma^{sat}} \xi(T^{sat}) \tag{38}$$

$$\frac{\sigma - \sigma^{sat}}{\sigma^{sat}} \simeq \nabla T (h^{sat})^2 \frac{\rho_l^{sat} + \rho_v^{sat}}{2} \frac{\rho_v^{sat} \mathcal{L}}{2T^{sat}\left(\rho_l^{sat} - \rho_v^{sat}\right)\sigma^{sat}} \xi(T^{sat}), \tag{39}$$

where

$$\xi(T) \hat{=} \frac{2\rho_l^{sat}}{\rho_l^{sat} - \rho_v^{sat}} \ln\left(\frac{2\rho_l^{sat}}{\rho_l^{sat} + \rho_v^{sat}}\right) - 1. \tag{40}$$

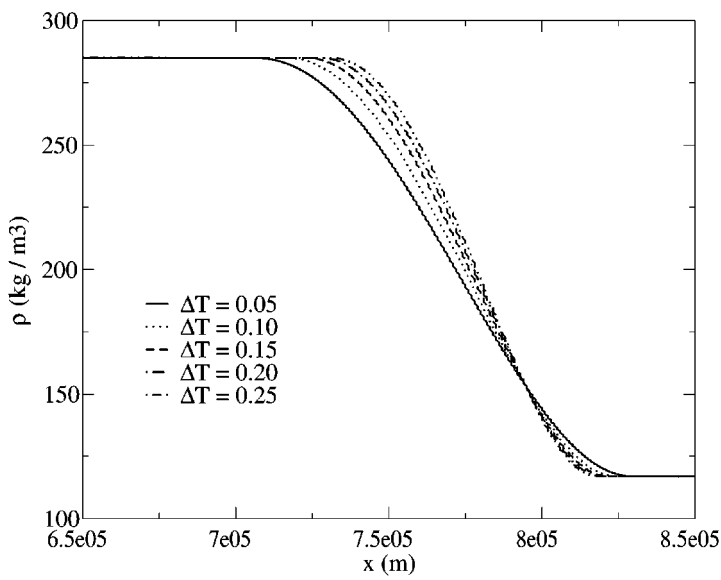

FIG. 9. Density profiles across an artificial enlarged liquid–vapor interface ($h^{sat} = 10^{-5}$ m) at mechanical equilibrium crossed by increasing heat fluxes.

Equations (38) and (39) show that *the relative variation of the interface thickness and the surface tension is linear in the temperature gradient within the interfacial zone and quadratic in the interface thickness at equilibrium*. These variations are therefore more sensitive to the interface thickness at equilibrium than they are in the presence of a mass flux. Jamet [15] showed that Eqs. (38) and (39) give the right dependencies on ∇T and h^{sat} but that the proportionality factor is underestimated by a factor 2 to 3 for water.

As an illustrative example, let us suppose that, for any reason, it is acceptable to make a relative error of 1% on the value of the surface tension. At 1 K below the critical point, for the problem sketched in Fig. 7, the temperature gradient in the vicinity of the interface must be lower than 0.65 K m^{-1}, which would correspond to a maximum value of the conductive heat flux across the superheated vapor and the subcooled liquid equal of about 0.2 W m^{-2} and an artificial interface thickness of 10^{-5} m. If this value is considered to be too small for the physical parameters used in the numerical simulation intended, the only solution is to increase the mesh resolution to support a decreased artificial interface thickness.

This feature can sometimes be a limitation. For instance, in the simulation considered in [38, p. 673], the present method could be used with an interface thickness at most equal to 0.25 mm if the relative error on the surface tension had to be less than 1%. The second gradient method would have required a mesh spacing about 10 times smaller than the one used in [38] with the most refined resolution, which would be prohibitive with no local mesh refinement.

5. APPLICATIONS

In this section, illustrative examples of preliminary results using the method presented in the previous sections are presented. Although they do not cover all the potential uses of the method, they are considered to be test cases before a complete simulation of a liquid–vapor flow with phase change can be performed. A one-dimensional liquid–vapor phase-change problem is illustrated in Section 5.1; two-dimensional problems are presented in Section 5.2.

5.1. *One-Dimensional Phase-Change Problem*

The solution to the problem considered (see Fig. 10) requires the resolution of the three balance equations (6), (7), and (8). To stress the importance of the change in thermodynamics introduced in Section 3, the results obtained for the classical van der Waals' equation of state will be compared to those obtained for a modified equation of state. It must be emphasized that the size of the physical domain is very different depending on whether the equation of state is modified or not, since the size of the domain is proportional to the interface thickness for a roughly constant computational time. In addition, even in the vicinity of the critical point, the physical interface thickness is very small and the size of the domain must therefore be very small. In contrast, the use of the modified thermodynamics presented in

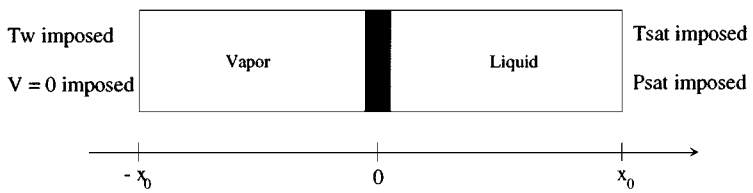

FIG. 10. Sketch of a one-dimensional vaporization problem.

Section 3 allows the interface thickness to be chosen as an independent parameter (provided that limitations exhibited in Section 4 are acceptable) and the size of the domain can *a priori* be chosen arbitrarily.

The fluid is water and the saturation temperature is equal to 646.3 K, i.e., $T^{sat} = T_c - 1\,\mathrm{K}$. The results with a modified equation of state presented in the following are such that $h^{sat} = 0.1$ mm and $x_0 = 2$ mm. The artificial enlargement is thus close to 625.

The set of initial conditions for the computations presented in this section are the following:

- There is a zero velocity field on the whole domain.
- There is a linear temperature field from $T_w = T^{sat} + \Delta T$ at $x = -x_0$ to T^{sat} at $x = 0$, with constant temperature T^{sat} from $x = 0$ to $x = +x_0$ and $\Delta T = +0.6$ K.
- The density fields in the vapor phase (from $x = -x_0$ to $x = 0$) and the liquid phase (from $x = 0$ to $x = +x_0$) are first computed by modeling the interface as a discontinuity and the profile is then smoothed in the vicinity of the interface (approximately from $x = -h^{sat}/2$ to $x = +h^{sat}/2$) to recover the equilibrium thickness dictated by the second gradient formulation; this initial density profile does not correspond perfectly to the equilibrium state but nevertheless leads to a decent initial transient.

Equations (6)–(8) are solved using a classical MAC scheme in space and a first-order explicit Euler scheme in time. Special attention is paid to the boundary conditions for which we adapted the NSCBC approach of Thompson [35] and Poinsot *et al.* [28] to impose the boundary conditions prescribed in Fig. 10.

The results will be presented in a nondimensional form, introducing the following simple scaling.

- For the sake of convenience, a characteristic conduction time derived from the vapor Fourier number is used for the time scale;

$$\tau_c \hat{=} \frac{\rho_v^{sat}(2x_0)^2 Cp_v}{k_v}, \tag{41}$$

where ρ_v^{sat}, Cp_v, and k_v are evaluated at $T^{sat} = 646.3$ K.
- The length scale is chosen to be x_0.
- The velocity scale is therefore x_0/τ_c. This choice allows the results to be of order one.

The reduced quantities x^*, t^*, and V^* that will be used in the following are respectively defined as $x^* \hat{=} x/x_0$, $t^* \hat{=} t/\tau_c$, and $V^* \hat{=} V/x_0$.

Figure 11 shows the density, velocity, and temperature profiles at the reduced times t^* equal to $0, 0.1, 0.2, 0.3, \ldots$. It is seen that the liquid is pushed out of the computational domain by the vapor produced at the interface. Figure 11b shows that, after a short transient, the velocity in the bulk phases is fairly uniform (slightly modified by the thermal expansion in the vapor phase), whereas the velocity jump corresponding to the vaporization process is smoothed across the interface thickness.

Figure 12 gives a comparison between the reduced interface position $x_i^* \hat{=} x_i/x_0$ as a function of the reduced time, calculated from the results of Fig. 11a and the one obtained by an analytical model of a discontinuous interface.

In the analytical model, it is assumed that the interface is discontinuous and that the Péclet number is negligible. This last assumption is not completely valid in our example:

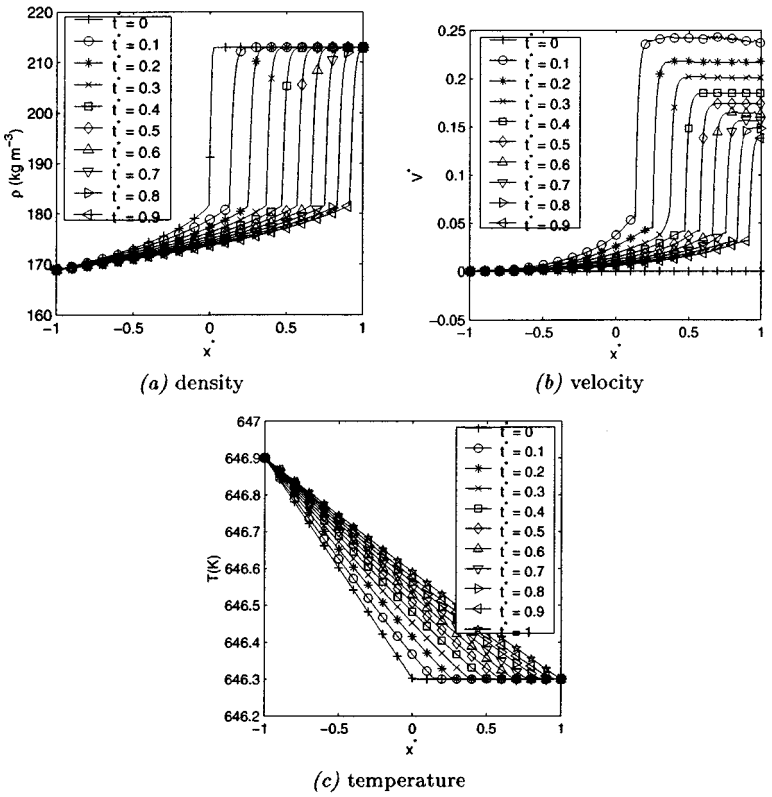

(a) density *(b)* velocity

(c) temperature

FIG. 11. One-dimensional problem: Reduced time sequence ($t^* = 0, 0.1, 0.2, 0.3, \ldots$) of the density, velocity, and temperature fields versus the reduced space coordinate x^*.

if the physical properties are estimated using $(\rho_v^w + \rho_v^{sat})/2$ and $(T_w + T^{sat})/2$, the Péclet number

$$Pe \hat{=} \frac{Cp\Delta T}{\mathcal{L}} \simeq 0.47 \tag{42}$$

is indeed not negligible, and that gives a good explanation to the slight discrepancies between the analytical results for $Pe = 0$ and the numerical results given in Fig. 12. Indeed, the

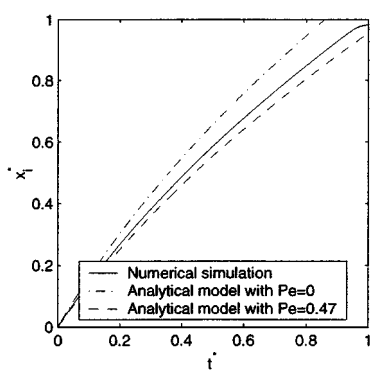

FIG. 12. One-dimensional problem: Comparison of the numerical results with an analytical model showing evolution of the reduced position of the interface x_i^* versus the reduced time t^*.

first-order correction accounting for a nonzero Péclet number is given by an apparent latent heat of vaporization $\mathcal{L}_{Pe}$ defined as

$$\mathcal{L}_{Pe} \hat{=} \mathcal{L}\left(1 + \frac{1}{2}Pe\right), \tag{43}$$

where the Péclet number is estimated to be constant throughout the entire vapor phase ($Pe = 0.47$).

This correction accounts for the heat-capacity effect in the vapor phase, which is decreased when the temperature gradient decreases due to the motion of the interface. Figure 12 shows that the correction term has the proper order of magnitude, even though the correction is not perfect, probably because of the variation of Cp with temperature.

Owing to the nonlinear effects induced by the variation of the Péclet number in space and time, the numerical results reported in Fig. 12 can be considered satisfactory compared to an approximate analytical solution. Note that these good results are obtained even though the interface was artificially enlarged.

5.2. *Examples of Two-Dimensional Isothermal Flows*

In this section, results of two-dimensional simulations will be presented. A first study will be dedicated to the numerical convergence of the Laplace relation. The other applications are unsteady. However, for the sake of simplicity, isothermal systems are considered. It must be emphasized that, *even though the systems are isothermal, phase change exists*, as explained in Section 4.2. However, since the systems considered are closed, phase change can only be local and is therefore limited.

5.2.1. Numerical convergence of the Laplace relation. The Laplace relation is the main macroscopic consequence of the existence of surface tension. With the proposed method, surface tension is transformed into a continuous force within an interfacial zone that is discretized with a finite number of grid points, and the convergence of the Laplace relation must therefore be addressed. Moreover, it is believed that this convergence analysis is the most important one in order to understand convergence issues on more macroscopic and coupled problems.

To perform this convergence analysis, the following parameters were chosen:

- The fluid is water,
- The system is isothermal at a temperature equal to 646.3 K (1 K below the critical temperature),
- The system is two dimensional: a 2.7 mm by 2.7 mm square,
- The fluid mass is such that if the interface were a discontinuity, the radius of the vapor bubble would be equal to 1 mm,
- The surface tension, the vapor, and the liquid densities are approximately equal to 7×10^{-5} N/m, 182 kg/m^3, and 213 kg/m^3 respectively,
- The vapor and liquid phases are modeled by the van der Waals' equation of state,
- The artificial thickness of the interface is equal to 0.1 mm.

Once a steady state is reached, the pressure difference between the center of the bubble and the square corners is measured. Note that the steady state is not an equilibrium state since, with the numerical method used to discretize the equations of motion, parasitic currents are observed, which are similar in shape to those reported in [3] for instance.

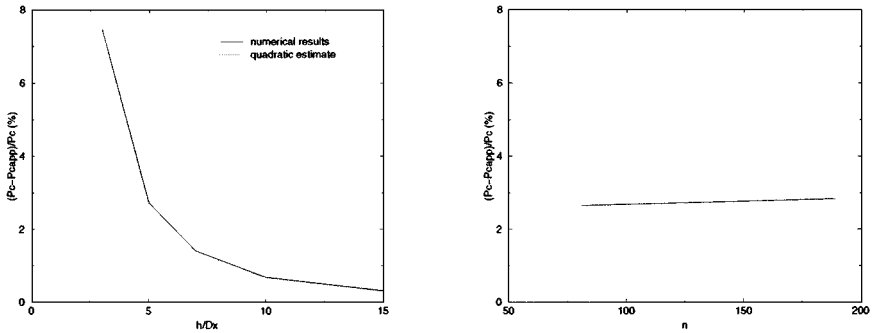

FIG. 13. Convergence of the Laplace relation. n, h, Dx, and Pc are, respectively, the number of grid points on one edge (n^2 is the total number of grid points), the interface thickness, the mesh size, and the capillary pressure ($Pcapp$ is the "measured" capillary pressure, whereas Pc is the theoretical capillary pressure.)

Since the interface thickness is a parameter that can be chosen, we performed two convergence studies. First, the interface thickness is fixed and the number of grid points is increased, thus increasing the number of grid points within the interface. Second, the number of grid points is increased but the number of grid points within the interface is kept constant, thus decreasing the artificial thickness of the interface. The results obtained are given in Fig. 13.

Figure 13a shows that the convergence of the Laplace relation with an increasing number of grid points within the interfacial zone is quadratic. In contrast, Fig. 13b shows that, when the number of grid points is increased without increasing the number of grid points within the interfacial zone, the Laplace relation does not converges and that the relative error is nearly a constant (with a slight increase). Therefore, it can be concluded that the error on the Laplace relation is due only to the truncation error introduced within the interfacial zone.

Note that other numerical results, not reported here, showed that the pressure difference is proportional to the inverse of the bubble radius and that the error on the Laplace relation does not depend on the bubble radius.

5.2.2. Coalescence of two bubbles in the absence of gravity. In this section, we present the ability of the method proposed to deal with topology changes. Figure 14 shows the time evolution of two two-dimensional bubbles initially separated but nevertheless very close to each other. It can be seen that very rapidly the two bubbles coalescence and that the single bubble thus created finally reaches an equilibrium state. The density fluctuations observed in the phases in the early stages of the coalescence are due to the pressure waves generated during the process.

Even though the initial coalescence behavior certainly depends on the interface thickness and on the numerical discretization, it must be emphasized that the change in the topology is made at absolutely no cost. This property will be kept at no cost in three dimensions. The influence of the numerical parameters on coalescence and breakup will be investigated in the future.

It must be noticed that to be able to obtain this coalescence in a quiescent liquid, the bubbles have to be very close to each other (i.e., of the order of the interface thickness). Indeed, if the bubbles are too far apart, it is observed that the smaller one shrinks and

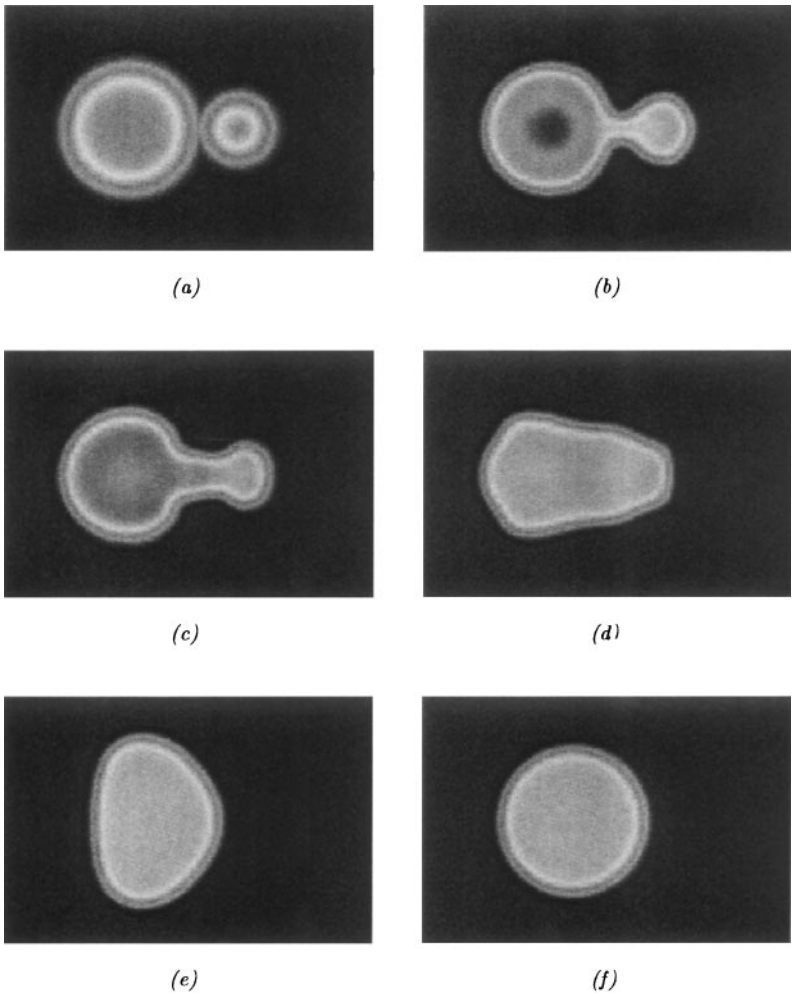

FIG. 14. Time sequence of the coalescence of two bubbles initially at rest in microgravity (low density in light and high density in dark). Fluid: water; $T = 646.3$ K; equation of state: van der Waals; $\lambda = 1.773 \times 10^{-14}$ Pa m^8 kg^{-3}; 4.2×2.8 μm rectangle; 316×210 grid; radii of the initial bubbles: 0.7 and 0.35 μm..

disappears while the bigger one grows accordingly. Thus no coalescence is observed. This behavior can be explained thermodynamically. It is well known that the equilibrium of a bubble in an isothermal and isobaric system is unstable (e.g., [5]); i.e., if the radius is slightly greater than the equilibrium radius, the bubble grows endlessly and if it is slightly smaller than the equilibrium radius, the bubble shrinks and disappears. It then appears that in the closed system considered here, the bigger bubble imposes its pressure in the liquid: the pressure outside the smaller bubble is bigger than the equilibrium pressure for the smaller bubble, which then shrinks.

It must be emphasized that the physical features of the coalescence simulated here are limited to the model considered and that no attempt has been made to account for physical effects that affect the coalescence such as electrical interactions [8, 20, 26].

Spinodal decomposition is also a good example of large topology changes. Numerical simulations of spinodal decomposition using the van der Waals' theory are reported in the literature [17, 25].

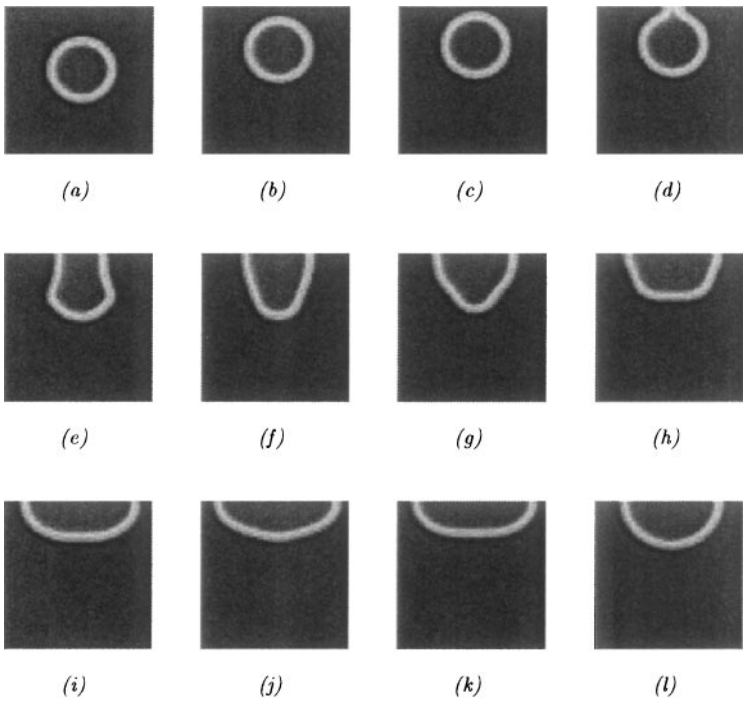

FIG. 15. Time sequence of the impact of a rising bubble initially at rest on a wall. Fluid: water; $T = 646.3$ K; equation of state: van der Waals; $\lambda = 1.773 \times 10^{-14}$ Pa m^8 kg^{-3}; 2.5×2.5 μm square; 100×100 grid; contact angle: 90°.

5.2.3. Static contact angle. In this section, we show the ability of the method proposed to account for contact angles. The contact angle statics and dynamics described by the second gradient theory have already been studied theoretically by Seppecher [33]. The goal here is just to show through some numerical examples that some important physical features are recovered numerically by the second gradient method.

Figure 15 shows the time evolution of a bubble rising toward a wall under the action of gravity. For the sake of simplicity, a van der Waals' equation of state has been used.

It can be seen that the initial contact, as well as the evolution of the bubble once attached on the wall, can be captured. This is an important feature of our method since, to our knowledge, only one method is able to simulate a contact angle and a moving contact line in a rather general and numerically convenient way, this method being based on a similar theory [14]. It is observed that immediately after the contact of the bubble with the wall, the contact line moves very rapidly (with respect to the velocity of the bubble before the contact), which is what is commonly observed. Afterwards the surface tension plays its role by preventing the contact line from moving too far and an equilibrium state is reached in which the bubble has a hemicylindrical shape.

In the present simulation, a constant value of the contact angle is imposed by the simple boundary condition

$$\boldsymbol{n} \cdot \nabla \rho = 0, \tag{44}$$

where $\boldsymbol{n}$ is the unit normal to the boundary (i.e., the upper wall).

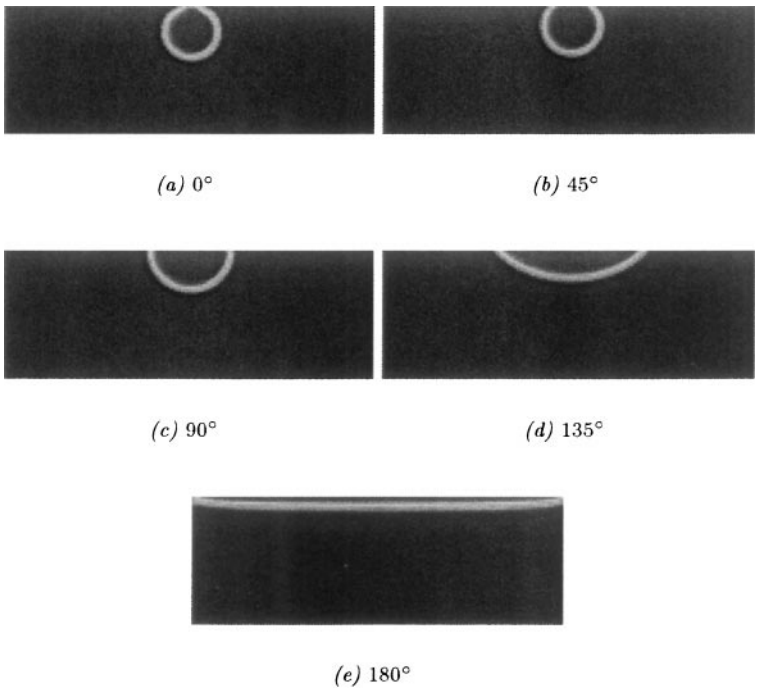

FIG. 16. Equilibrium shape of bubbles after their impact on a wall. Fluid: water; $T = 646.3$ K; equation of state: van der Waals; $\lambda = 1.773 \times 10^{-14}$ Pa m^8 kg^{-3}; 5×1.5 μm rectangle; 200×60 grid; contact angle: from 0 to 180°.

This condition imposes that the contact angle is equal to 90°, which is what is actually observed in Fig. 15, particularly in the last frame corresponding to the equilibrium state.

No contact angle variation with the speed of displacement of the contact line was introduced in this simulation. Seppecher [33] showed that this dependence can be correctly captured by the second gradient theory. However, this dependence may be affected the artificial thickening of the interface introduced for numerical purposes. This issue will be addressed in the future.

Figure 16 shows different equilibrium shapes of a bubble attached on a wall corresponding to different contact angles. These equilibrium states were obtained by performing the same simulation as the one presented in Fig. 15, in which the boundary condition (44) has been adapted to account for the desired contact angle.

It can be seen that any boundary behavior can be simulated, from a completely wetting material, where the bubble remains almost cylindrical (the wall has no affinity for the vapor), to a completely nonwetting one, where the bubble tends to spread completely (the wall has no affinity for the liquid). All the intermediate behaviors can be simulated as well, as shown in Fig. 16.

5.2.4. Contact angle hysteresis. Contact angle hysteresis is an important feature of a moving contact line. Experimentally, it is observed that when a gas–liquid interface in contact with a solid wall moves in the direction oriented from the liquid to the gas, the contact angle θ_a is greater than the contact angle θ_r observed when the interface moves in the opposite direction. These so-called advancing and receding contact angles are such that $\theta_r < \theta_{eq} < \theta_a$, where θ_{eq} is the contact angle at equilibrium (Fig. 17). Contact angle

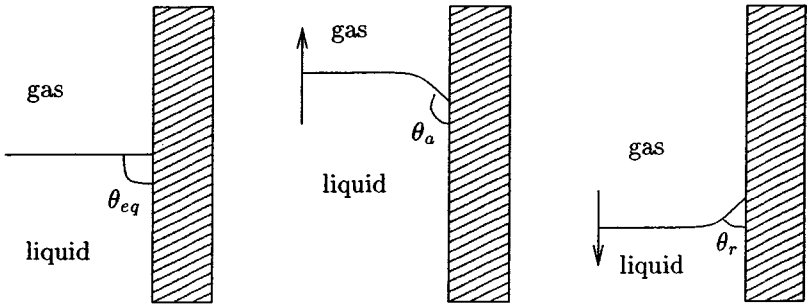

FIG. 17. Contact angle hysteresis.

hysteresis is at the origin of several common observations such as the fact that a droplet on an inclined wall does not always trickle down but reaches an equilibrium state or that some liquid can be sustained in a capillary tube despite gravity.

The origin of this hysteresis is still extensively studied and remains a subject of debate. However, the classical explanation is a consequence of a rough and/or chemically nonhomogeneous wall, which results in a *macroscopic* variation of the contact angle, its *microscopic* value being imposed by the local affinity of the wall for the fluid. Indeed, when a droplet moves on a chemically nonhomogeneous wall (Fig.18), for hydrodynamic stability reasons, the "advancing" contact line tends to keep in contact with the material whose contact angle is the greater, while the "receding" contact line tends to keep in contact with the material whose contact angle is the lower. Given the general shape of the droplet in Fig. 18, if the advancing contact angle were θ_r, the interface would be locally convex. The Laplace relation would induce a pressure gradient in the liquid such that the advancing contact line would be pushed forward until the contact angle is back θ_a. Therefore, the advancing contact line tends to be more in contact with the material whose contact angle is θ_a than the other and the time-averaged advancing contact angle (the one observed) is closed to θ_a. The same reasoning can be applied to the "receding" contact line (see [5, p. 76] for further details).

Imposing a chemically nonhomogeneous boundary is particularly easy in the second gradient method: the boundary condition (44) must vary spatially, as shown in Fig. 18 where the contact angle is a piecewise constant function of space. However, for numerical convenience, this function is chosen to be more regular,

$$\theta(x) = \theta_{eq} + \Delta\theta \cos\left(2\pi \frac{x}{d}\right), \tag{45}$$

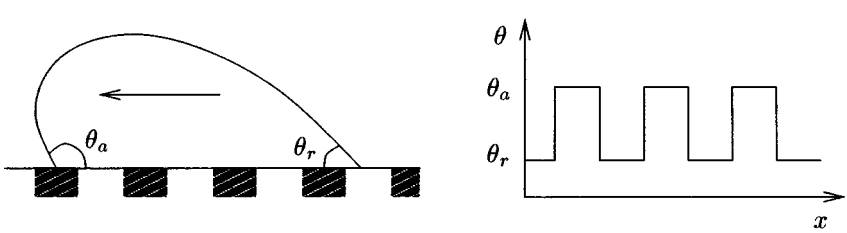

FIG. 18. Sketch of a droplet moving from the right to the left on a wall made of two materials, whose equilibrium contact angles are θ_a and θ_r, respectively.

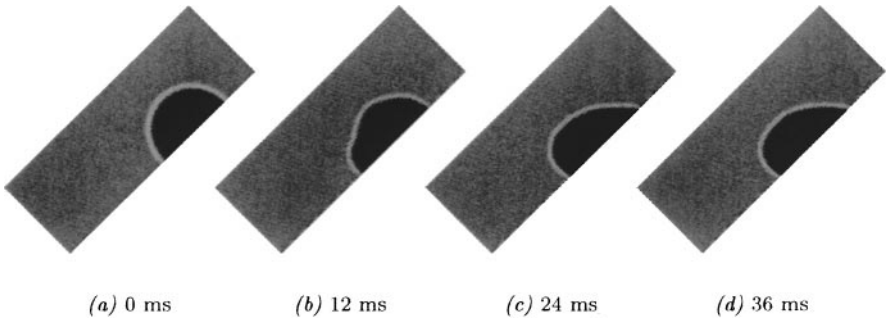

FIG. 19. Time sequence of the evolution of a drop on an inclined wall (45°). Last picture corresponds to the equilibrium state. Fluid: water; $T = 618.8$ K; $\rho_v = 103$ kg m^{-3}; $\rho_l = 592$ kg m^{-3}; $\sigma = 4.66 \times 10^{-3}$ N m^{-1}; equation of state: modified such that $h = 0.1$ mm; $\lambda = 2.83 \times 10^{-12}$ Pa m^8 kg^{-3}; 6×2 mm rectangle; 300×100 grid; initial diameter: 2 mm; gravity: 9.81 m s^{-2}.

where θ_{eq} is the equilibrium contact angle, d is a distance of the order of the interface thickness (at least equal to $2\,h$), and $\Delta\theta$ is the amplitude of the contact angle variation.

The boundary condition (44) is therefore replaced by

$$\boldsymbol{n} \cdot \nabla\rho = \frac{\sigma}{\lambda(\rho_l - \rho_v)} \cos[\theta(x)]. \tag{46}$$

Imposing such a boundary condition, we can numerically solve for the time evolution of a droplet on a inclined wall, and these results are presented in Fig. 19. The wall properties of this computation are such that $\theta_{eq} = 90°$, $d = 4\,h$, and $\Delta\theta = 45°$. It is observed that the contact lines move erratically, which corresponds to the physical explanation of the contact angle hysteresis presented above. This erratic movement is at the origin of the capillary wave observed on the interface in the Fig. 19b that was created by the fast movement of the advancing contact line that then stopped moving for a while. The last frame is the equilibrium state obtained, which corresponds to what is commonly observed.

6. CONCLUSIONS AND PERSPECTIVES

In this paper, we have shown how the second gradient theory could be used for the numerical simulation of liquid–vapor flows with phase change. We have in particular established the equations of evolution of a fluid endowed with internal capillarity by using the principle of virtual work, which we consider to be the most coherent way to derive these equations. Once the equations have been formally established, the numerical application of this theory has been addressed. In particular it is shown that the thermodynamic behavior of the fluid must be modified and the interfaces must be artificially enlarged. Then the interfaces can be resolved by a grid of reasonable size, without changing the surface tension. We show that the function $P(\rho)$ must display strong variation near the binodal curve in order not to change the sound speed within the phases and to keep some thermodynamic relations between the pressures inside and outside an inclusion at equilibrium.

It is also shown that, according to the second gradient theory, the thickness of an interface as well as its surface tension are functions of the mass flux and the temperature gradient across the interface. These variations are shown to increase with the thickness of the interface, which means that limited heat and mass transfers across an interface can be

simulated using this method. However, we emphasize that these limitations are reasonably well understood and that some adaptations could therefore be developed in the future to avoid these limitations.

Despite these limitations, we have shown through various examples of applications that the method can be successfully used in one as well as two dimensions. We believe that the main advantages of the method presented are that it has a clear and strong theoretical justification and that topological changes and moving contact lines are handled very easily. Moreover, going from two dimensions to three dimensions is straightforward compared to other methods.

Nevertheless, work still has to be done to make sure that this method can be accurately applied in a wide range of applications. In addition, other more fundamental issues will also be addressed such as the influence of the enlargement of the interface on the contact line motion and the dependence of the results on the numerical resolution and the interface thickness.

ACKNOWLEDGMENTS

We are indebted to Professor Henri Gouin, Université d'Aix-Marseille, for the very helpful discussions with us in our first struggles with the second gradient theory. We are also very thankful to Jerry Brackbill, Los Alamos National Laboratory, for the helpful suggestions he made concerning this manuscript.

REFERENCES

1. D. M. Anderson, G. B. McFadden, and A. A. Wheeler, Diffuse-interface models in fluid mechanics, *Annu. Rev. Fluid Mech.* **30**, 139 (1998).
2. Z. Bi and R. F. Sekerka, Phase-field model of solidification of a binary alloy, *Physica A* **261**, 95 (1998).
3. J. U. Brackbill, D. B. Kothe, and C. Zemach, A continuum method for modeling surface tension, *J. Comput. Phys.* **100**, 335 (1992).
4. J. W. Cahn and J. E. Hilliard, Free energy of a nonuniform system. I. Interfacial free energy, *J. Chem. Phys.* **28**(2), 258 (1958).
5. V. P. Carey, *Liquid–Vapor Phase-Change Phenomena: An Introduction to the Thermophysics of Vaporisation and Condensation Processes in Heat Transfer Equipment* (Hemisphere Publishing Washington, DC, 1992).
6. P. Casal and H. Gouin, Relation entre l'équation de l'énergie et l'équation du mouvement en théorie de Korteweg de la capillarité, *C. R. Acad. Sci. Paris* **300**(7), 231 (1985).
7. P. Casal and H. Gouin, Sur les interfaces liquide-vapeur non isothermes, *J. Méc. Théorique Appliquée* **7**(6), 689 (1988).
8. A. K. Chesters, The modeling of coalescence processes in fluid-liquid dispersions: A review of the current understanding, *Trans. IChemE* **69**(A), 259 (1991).
9. J. M. Delhaye, Jump conditions and entropy sources in two-phase systems. Local instant formulation, *Int. J. Multiphase Flow* **1**, 395 (1974).
10. F. Dell'Isola, H. Gouin, and G. Rotoli, Nucleation of spherical shell-like interfaces by second gradient theory: Numerical simulations, *Eur. J. Mech. B/Fluids* **15**(4), 545 (1996).
11. H. Gouin and J. M. Delhaye, Material waves of a fluid in the vicinity of the critical point, in edited by S. Morika and L. van Wijngaarden *IUTAM Symposium on Waves in Liquid/Gas and Liquid/Vapour Two-Phase Systems*, (Kluwer Academic Publishers, Dordrecht, 1995), p. 405.
12. M. Ishii, *Thermo-Fluid Dynamic Theory of Two-Phase Flow* (Eyrolles, Paris, 1975).
13. D. Jacqmin, An energy approach to the continuum surface tension method, in *Proceedings of the 34th Aerospace Sciences Meeting and Exhibit, 1996.* AIAA 96-0858.
14. D. Jacqmin, Calculation of two-phase Navier–Stokes flows using phase-field modeling, *J. Comput. Phys.* **155**, 1 (1999).

15. D. Jamet, *Etude des potentialites de la théorie du second gradient pour la simulation numérique directe des écoulements liquide-vapeur avec changement de phase*, Ph.D. thesis (Ecole Central Paris, 1998).
16. D. Jamet, O. Lebaigue, N. Coutris, and J. M. Delhaye, A numerical description of a liquid-vapor interface based on the second gradient theory, *Fluid Mech. Res.* **22**(1), 1 (1997).
17. D. Jasnow and J. Viñals, Coarse-grained description of thermo-capillary flow, *Phys. Fluids* **8**, 660 (1996).
18. D. Juric, *Computations of Phase Change*, Ph.D. thesis (University of Michigan, 1996).
19. D. Juric and G. Tryggvason, Computations of boiling flows, *Int. J. Multiphase Flow* **24**(3), 387 (1998).
20. N. I. Kolev, Fragmentation and coalescence dynamics in multiphase flows, *Exp. Thermal Fluid Sci.* **6**, 211 (1993).
21. D. J. Korteweg, Sur la forme que prennent les équations du mouvement des fluides si l'on tient compte des forces capillaires causées par des variations de densité considérables mais continues et sur la théorie de la capillarité dans l'hypothèse d'une variation continue de la densité, *Arch. Néerl. Sci. Exactes Nat.* **6**, 1 (1901).
22. B. Lafaurie, C. Nardone, R. Scardovelli, S. Zaleski, and G. Zanetti, Modelling merging and fragmentation in multiphase flows with SURFER, *J. Comput. Phys.* **113**, 134 (1994).
23. J. C. Maxwell, On the dynamical evidence of the molecular constitution of bodies, *Nature* **11**, 357 (1875).
24. G. B. McFadden, A. A. Wheeler, R. J. Braun, and S. R. Coriell, Phase-field models for anisotropic interfaces, *Phys. Rev. E* **48**(3), 2016 (1993).
25. B. T. Nadiga and S. Zaleski, Investigations of a two-phase fluid model, *Eur. J. Mech. B/Fluids* **15**(6), 885 (1996).
26. T. Palermo, Le phénomène de coalescence, *Rev. Inst. Français Pétrole* **46**(3), 325 (1991).
27. O. Penrose and P. C. Fife, Thermodynamically consistent models of phase-field type for kinetics of phase transitions, *Physica D* **43**, 44 (1990).
28. T. J. Poinsot and S. K. Lele, Boundary conditions for direct simulations of compressible viscous flows, *J. Comput. Phys.* **101**, 104 (1992).
29. J. M. Reese, L. C. Woods, F. J. P. Thivet, and S. Candel, A second-order description of shock structure, *J. Comput. Phys.* **117**, 240 (1995).
30. Y. Rocard, *Thermodynamique* (Masson, Paris, 1967).
31. J. S. Rowlinson and B. Widom, *Molecular Theory of Capillarity* (Oxford University Press, New York, 1982).
32. P. Seppecher, *Etude d'une modélisation des zones capillaires fluides: Interfaces et lignes de contact*, Ph.D. thesis (Université Paris VI, 1987).
33. P. Seppecher, Moving contact line in the Cahn–Hilliard theory, *Int. J. Eng. Sci.* **34**(9), 977 (1996).
34. J. A. Sethian, *Level Set Methods* (Cambridge University Press, Cambridge, UK, 1996).
35. K. W. Thompson, Time dependent boundary conditions for hyperbolic systems, *J. Comput. Phys.* **68**, 1 (1987).
36. S. O. Unverdi and G. Tryggvason, A front-tracking method for viscous, incompressible, multi-fluid flows, *J. Comput. Phys.* **100**, 25 (1992).
37. van der Waals, Thermodynamische Theorie der Kapillarität unter Voraussetzung stetiger Dichteanderung, *Z. Phys. Chem.* **13**, 657 (1894). English translation in *J. Stat. Phys.* **20**, 197 (1979).
38. S. W. J. Welch and J. Wilson, A volume of fluid based method for fluid flows with phase change, *J. Comput. Phys.* **160**, 662 (2000).
39. A. A. Wheeler, B. T. Murray, and R. J. Schaefer, Computation of dendrites using a phase field model, *Physica D* **66**, 243 (1993).